



Deposited via The University of Sheffield.

White Rose Research Online URL for this paper:

<https://eprints.whiterose.ac.uk/id/eprint/207701/>

Version: Published Version

Article:

The LVK Collaboration (2023) Search for subsolar-mass black hole binaries in the second part of Advanced LIGO's and Advanced Virgo's third observing run. Monthly Notices of the Royal Astronomical Society, 524 (4). pp. 5984-5992. ISSN: 0035-8711

<https://doi.org/10.1093/mnras/stad588>

Reuse

This article is distributed under the terms of the Creative Commons Attribution (CC BY) licence. This licence allows you to distribute, remix, tweak, and build upon the work, even commercially, as long as you credit the authors for the original work. More information and the full terms of the licence here:

<https://creativecommons.org/licenses/>

Takedown

If you consider content in White Rose Research Online to be in breach of UK law, please notify us by emailing eprints@whiterose.ac.uk including the URL of the record and the reason for the withdrawal request.

Search for subsolar-mass black hole binaries in the second part of Advanced LIGO’s and Advanced Virgo’s third observing run

The LVK Collaboration[★]

Laser Interferometer Gravitational-Wave Observatory, 127124 N Route 10, Richland, WA 99354, USA

Accepted 2023 February 13. Received 2023 February 10; in original form 2022 December 22

ABSTRACT

We describe a search for gravitational waves from compact binaries with at least one component with mass $0.2\text{--}1.0 M_{\odot}$ and mass ratio $q \geq 0.1$ in Advanced Laser Interferometer Gravitational-Wave Observatory (LIGO) and Advanced Virgo data collected between 2019 November 1, 15:00 UTC and 2020 March 27, 17:00 UTC. No signals were detected. The most significant candidate has a false alarm rate of 0.2 yr^{-1} . We estimate the sensitivity of our search over the entirety of Advanced LIGO’s and Advanced Virgo’s third observing run, and present the most stringent limits to date on the merger rate of binary black holes with at least one subsolar-mass component. We use the upper limits to constrain two fiducial scenarios that could produce subsolar-mass black holes: primordial black holes (PBH) and a model of dissipative dark matter. The PBH model uses recent prescriptions for the merger rate of PBH binaries that include a rate suppression factor to effectively account for PBH early binary disruptions. If the PBHs are monochromatically distributed, we can exclude a dark matter fraction in PBHs $f_{\text{PBH}} \gtrsim 0.6$ (at 90 per cent confidence) in the probed subsolar-mass range. However, if we allow for broad PBH mass distributions, we are unable to rule out $f_{\text{PBH}} = 1$. For the dissipative model, where the dark matter has chemistry that allows a small fraction to cool and collapse into black holes, we find an upper bound $f_{\text{DBH}} < 10^{-5}$ on the fraction of atomic dark matter collapsed into black holes.

Key words: black hole physics – dark matter – black hole mergers.

1 INTRODUCTION

The Advanced Laser Interferometer Gravitational-Wave Observatory (LIGO; Aasi et al. 2015) and Advanced Virgo (Acernese et al. 2015) detectors have completed three observing runs, O1, O2, and O3 (split into O3a and O3b), since the first observation of gravitational waves (GWs) from a binary black hole (BBH) coalescence (Abbott et al. 2016b). The collected data have been analysed by the LIGO–Virgo–KAGRA (LVK) Collaboration (Abbott et al. 2020a) in successive versions of the Gravitational-Wave Transient Catalog (GWTC; Abbott et al. 2016a, 2019a, 2021a,b,c), which report a total of 90 candidates GW events from the coalescence of compact binary systems with a probability of astrophysical origin >0.5 . Several additional candidates of compact binary signals have also been included in independent catalogues (Magee et al. 2019; Nitz et al. 2019a,b, 2023, 2021; Venumadhav et al. 2019, 2020; Olsen et al. 2022) after analysing the publicly released strain data (Abbott et al. 2021d). These detections have revealed features in the population of coalescing objects that revolutionize our previous understanding of astrophysics and stellar evolution (Mandel & Farmer 2022; Spera, Trani & Mencagli 2022). The masses of many black holes (BHs) detected in GWs are much larger than those of the BHs observed in X-ray binaries (Bailyn et al. 1998; Ozel et al. 2010; Farr et al. 2011; Fishbach & Kalogera 2022) and some signals, such as GW190521 (Abbott et al. 2020c,f), have primary component masses

within the predicted pair-instability mass gap (Woosley 2017; Farmer et al. 2019). On the other side of the mass range are events like GW190425 (Abbott et al. 2020d), whose total mass is substantially larger than any known Galactic neutron star binary (Farrow, Zhu & Thrane 2019; Abbott et al. 2020b), and events like GW190814 (Abbott et al. 2020e, 2021e) and GW200210_092254 (Abbott et al. 2021b) that are also atypical due to their highly asymmetric masses and the properties of their light components (Zevin et al. 2020). While open questions remain, GWs have provided a unique census of the population of BHs in binaries in our Universe (Abbott et al. 2023).

Current models of stellar evolution predict that white dwarfs that end their thermonuclear burning with a mass greater than the Chandrasekhar limit (Chandrasekhar 1931, 1935; Suwa et al. 2018; Müller et al. 2019; Ertl et al. 2020) will collapse to form either a neutron star or a supersolar-mass BH. Since there are no standard astrophysical channels that produce subsolar-mass (SSM) objects more compact than white dwarfs, the detection of an SSM compact object would indicate the presence of a new formation mechanism alternative to usual stellar evolution.

Given the still unknown nature of 84 per cent of the matter in the Universe (Aghanim et al. 2020), it is reasonable to consider whether the dark matter (DM) might be composed of, or produce, distinct populations of compact objects. Primordial black holes (PBHs), postulated to form from the collapse of large overdensities in the early Universe (Zel’dovich & Novikov 1967; Hawking 1971; Carr & Hawking 1974; Chapline 1975), are candidates to form at least a fraction of the DM while providing an explanation to

[★] E-mail: lvc.publications@ligo.org

several open problems in astrophysics and cosmology (Barrow et al. 1991; Bean & Magueijo 2002; Kashlinsky 2016; Clesse & García-Bellido 2018). Soon after the first BBH coalescence was observed, it was suggested (Bird et al. 2016; Sasaki et al. 2016; Clesse & García-Bellido 2017) that the detected BHs could have a primordial origin. Large primordial fluctuations at small scales generated during inflation can produce PBHs (Carr & Lidsey 1993; Ivanov, Naselsky & Novikov 1994; García-Bellido, Linde & Wands 1996; Kim & Lee 1996), though other processes in the early Universe, like bubble nucleation and domain walls (Garriga, Vilenkin & Zhang 2016), cosmic string loops, and scalar field instabilities (Khlopov, Malomed & Zeldovich 1985; Cotner & Kusenko 2017) can also be sources of overdensities that eventually collapse to produce PBHs (Khlopov 2010; Carr & Kühnel 2020; Carr et al. 2021b; Villanueva-Domingo, Mena & Palomares-Ruiz 2021). The thermal history of the Universe can further enhance the formation of PBH at different scales (Carr et al. 2021a). For example, the quark–hadron (QCD) transition significantly reduces the radiation pressure of the plasma, so that a uniform primordial enhancement stretching across the QCD scale will generate a distribution of PBH masses that is sharply peaked around a solar mass (Byrnes et al. 2018) and a broader mass distribution at both larger and smaller masses that could explain some of the GW observations (Jedamzik 2020, 2021; Chen, Yuan & Huang 2022; Clesse & García-Bellido 2022; Franciolini & Urbano 2022; Juan, Serpico & Franco Abellán 2022). In particular, GW events in the SSM range could be used to probe mergers involving PBHs from a QCD enhanced peak.

Models of particle DM can also produce compact objects either from an interaction of DM with Standard Model particles, such as boson stars or neutron stars transmuted into BHs due to DM accretion (Goldman & Nussinov 1989; de Lavallaz & Fairbairn 2010; Kouvaris & Tinyakov 2011; Bramante & Linden 2014; Bramante & Elahi 2015; Bramante, Linden & Tsai 2018; Kouvaris, Tinyakov & Tytgat 2018; Takhistov 2018; Dasgupta, Laha & Ray 2021; Takhistov, Fuller & Kusenko 2021), or directly from the gravitational collapse of dissipative DM (D’Amico et al. 2018; Shandera, Jeong & Gebhardt 2018; Chang et al. 2019; Choquette, Cline & Cornell 2019; Essig et al. 2019; Latif et al. 2019; Hippert et al. 2022; Ryan et al. 2022). DM black holes (DBHs) may form in the late universe if DM has a sufficiently rich particle content to allow dissipation and collapse of DM into compact structures. While these mechanisms generically produce BHs that overlap the standard astrophysical population, under specific assumptions they may also be able to create SSM compact objects.

Searches for compact binaries with at least one component below $1 M_{\odot}$ have been carried out using both Initial LIGO (Abbott et al. 2005, 2008), and Advanced LIGO and Advanced Virgo data (Abbott et al. 2018, 2019b, 2022; Nitz & Wang 2021a,b,c, 2022; Phukon et al. 2021). No firm detections were reported in any of these analyses. We describe and present the results of the search for the GWs from binary systems with at least one SSM component down to $0.2 M_{\odot}$, using data from the second part of the third observing run (O3b) in Section 2. We find no unambiguous GW candidates. The null result, combined with our previous analysis of the first part of the third observing run (O3a; Abbott et al. 2022), allows us to set in Section 3 upper limits on the merger rate of binaries with one SSM component, as function of the chirp mass and in the m_1 – m_2 plane.

These new upper limits on the merger rate can be used to constrain any model that might generate compact objects in the SSM range. As illustrative examples, we derive in Section 4 new constraints on two particular scenarios, PBHs and a model of DBHs. For PBH models, we calculate the merger rate of SSM binaries

taking into account the early (Hütsi et al. 2021) and late binary formation scenarios (Phukon et al. 2021; Clesse & García-Bellido 2022), and we re-evaluate the constraints on PBH DM models with monochromatic (δ -function) and extended mass distributions. We update the PBH merger rate model of previous LVK works (Abbott et al. 2018, 2019b, 2022) with additional physics to allow for binary disruption and find that the constraints on monochromatically distributed PBHs are weakened. We also consider broad PBH mass functions such as those of thermal history scenarios of PBHs and find that they are not significantly constrained in the SSM range by the present LVK data. For DBHs, we constrain a simple atomic DM model where DM consists of two oppositely charged dark fermions interacting via a dark photon (Shandera et al. 2018). This model has been estimated to produce a sizeable population of SSM BHs if the heavier of the fermions, X , is more massive than the Standard Model proton (Shandera et al. 2018); the fermion mass range previously probed was $0.66 < m_X < 8.8 \text{ GeV}/c^2$ (Singh et al. 2021; Abbott et al. 2022). We obtain improved constraints on the fraction of DM in DBHs as a function of the minimum mass of the DBHs. In Section 5, we summarize our findings and discuss prospects for Advanced LIGO and Advanced Virgo’s fourth observing run.

2 SEARCH

The SSM search analyses data collected during O3b, covering the period from 2019 November 1, 1500 UTC to 2020 March 27, 1700 UTC. The characterization and calibration of data and the non-linear removal of spectral lines follow the same methods as in our O3a analyses (Abbott et al. 2021a,c, 2022).

The analysis is performed by using three matched-filtering pipelines: GSTLAL (Messick et al. 2017; Sachdev et al. 2019; Hanna et al. 2020), MBTA (Aubin et al. 2021), and PyCBC (Allen 2005; Allen et al. 2012; Dal Canton et al. 2014; Usman et al. 2016; Nitz et al. 2017; Davies et al. 2020). These analyses correlate the data with a bank of templates that model the GW signals expected from binaries in quasi-circular orbit. All search pipelines use the same template banks and the same set-up as for the O3a SSM analysis (Abbott et al. 2022). Templates are generated using the TAYLORF2 waveform (Sathyaprakash & Dhurandhar 1991; Blanchet et al. 1995, 2005; Poisson 1998; Damour, Jaranowski & Schaefer 2001; Mikóczy, Vasuth & Gergely 2005; Arun et al. 2009; Buonanno et al. 2009; Bohé, Marsat & Blanchet 2013; Bohé et al. 2015; Mishra et al. 2016) and include phase terms up to 3.5 post-Newtonian order, but no amplitude corrections. We estimate the GW emission starting at a frequency of 45 Hz to limit the computational cost of the search; we estimate that this reduces the network average signal-to-noise ratio (SNR) by 7 per cent. The template bank was constructed using a geometric placement algorithm (Harry et al. 2014). The bank is designed to recover binaries with (redshifted) primary mass $m_1 \in [0.2, 10] M_{\odot}$ and secondary mass $m_2 \in [0.2, 1.0] M_{\odot}$. The lower mass bound is set for consistency with previous searches (Abbott et al. 2018, 2019b, 2022) and to limit the computational cost of the search. We additionally limit the binary mass ratio, $q \equiv m_2/m_1$, with $m_2 \leq m_1$, in the range $0.1 < q < 1.0$. We include the effect of spins aligned with the orbital angular momentum. For masses of a binary component larger than $0.5 M_{\odot}$ we allow for a dimensionless component spin ($\chi_{1,2} = |S_{1,2}|/m_{1,2}^2$, with $S_{1,2}$ the angular momentum of the compact objects) up to 0.9, while for compact objects with masses less than or equal to $0.5 M_{\odot}$, we limit the maximum dimensionless spin to 0.1. The restriction on component spins is chosen to reduce the computational cost of the analyses (Abbott et al. 2022). We set a

Table 1. The triggers with a false alarm rate (FAR) of $<2 \text{ yr}^{-1}$ in at least one search pipeline. We include the search-measured parameters associated with each candidate: m_1 and m_2 , the redshifted component masses, and χ_1 and χ_2 , the dimensionless component spin. The parameters shown in the table are the ones reported by the search where the trigger is identified with the lowest FAR. H, L, and V denote the Hanford, Livingston, and Virgo interferometers, respectively. The dashes in the ‘V SNR’ column mean that no single-detector trigger was found in Advanced Virgo. The network SNR is computed by adding the SNR of single-detector triggers in quadrature.

FAR (yr^{-1})	Pipeline	GPS time	m_1 (M_\odot)	m_2 (M_\odot)	χ_1	χ_2	H SNR	L SNR	V SNR	Network SNR
0.20	GstLAL	1267725971.02	0.78	0.23	0.57	0.02	6.31	6.28	–	8.90
1.37	MBTA	1259157749.53	0.40	0.24	0.10	−0.05	6.57	5.31	5.81	10.25
1.56	GstLAL	1264750045.02	1.52	0.37	0.49	0.10	6.74	6.10	–	9.10

minimum match (Owen 1996) of 0.97 to ensure that no more than 10 per cent of astrophysical signals can be missed due to the discrete sampling of the parameter space.

We report in Table 1 the most significant candidates down to the threshold false alarm rate (FAR) of $<2 \text{ yr}^{-1}$. We do not apply a trials factor to our analysis. We identify only three triggers that pass this threshold in at least one pipeline. Visual inspection of the data around the time of the triggers indicates no data quality issues that would point to a definitive instrumental origin of the candidates. However, the number of triggers with their estimated FAR is consistent with what we would expect if no astrophysical signal was present in the data, given that the duration of O3b is 0.34 yr and that three pipelines are being used. The most significant candidate has a FAR of 0.2 yr^{-1} , which assuming a Poisson distribution for the background triggers and an observing time of 0.34 yr, corresponds to a p -value of 6.6 per cent. We conclude that there is no statistically significant evidence for the detection of a GW from a SSM source.

3 SENSITIVITY AND RATE LIMITS

The absence of significant candidates in O3b allows us to characterize the sensitivity of our search and to set upper limits on the merger rate of such binary systems. We estimate the sensitive volume–time ($\langle VT \rangle$) over all of O3. We find the sensitivity of each of the three pipelines introduced in Section 2 with a common set of simulated signals in real data, generated using the precessing post-Newtonian waveform model SPINTAYLORT5 (Ajith 2011), with source component masses sampled from log-uniform distributions with primary masses in range $(0.19, 11.0) M_\odot$ and secondary masses in range $(0.19, 1.1) M_\odot$. The injection’s component spins are distributed isotropically with dimensionless spin magnitudes going up to 0.1. The injections are distributed uniformly in comoving volume up to a maximum redshift of $z = 0.2$, at which the sensitivity of the search has been checked to be negligible. We injected a total of approximately two million simulated signals, spaced 15 s apart, spanning all O3.

The sensitivity of each search pipeline is estimated by computing the sensitive volume–time of the search:

$$\langle VT \rangle = \epsilon V_{\text{inj}} T, \quad (1)$$

where ϵ is the efficiency, defined as the ratio of recovered to total injections in the data in the source frame mass bin of interest, T is the analysed time, and V_{inj} is the comoving volume at the farthest injected simulation. Each pipeline uses all injections with $q > 0.05$. We evaluate the uncertainties at 90 per cent confidence interval on the sensitive volume–time estimate (Tiwari 2018) and consider binomial errors on the efficiency ϵ , given by

$$\delta(VT) = 1.645 \sqrt{\frac{\epsilon(1-\epsilon)}{N_{\text{inj}}}} V_{\text{inj}} T, \quad (2)$$

where N_{inj} are the total injections in the considered mass range.

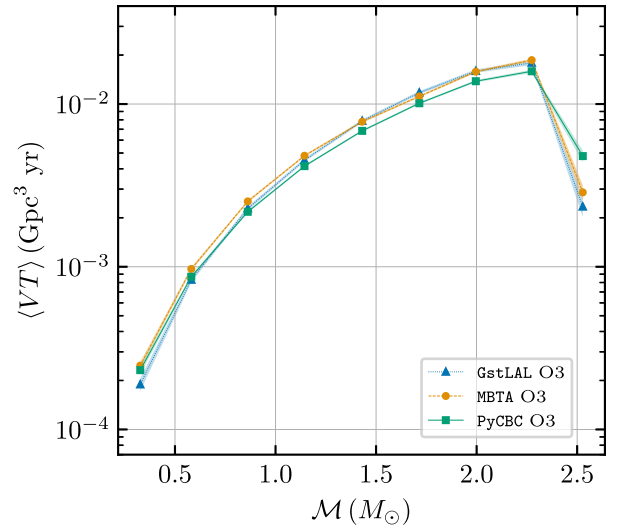


Figure 1. Sensitive volume–time as a function of the source frame chirp mass in data from O3, obtained through the analysis of the set of common injections (blue triangles with dotted lines, orange circles with dashed lines, and green squares with continuous lines). The statistical errors are evaluated at 90 per cent confidence interval, following equation (2) and represented by the shaded areas.

We use the FAR of the most significant candidate in O3 for each pipeline to estimate the upper limit on the merger rate in accordance with the loudest event statistic formalism (Biswas et al. 2009). The FAR thresholds used were 0.2, 1.4, and 0.14 yr^{-1} (Abbott et al. 2022) for GstLAL, MBTA, and PyCBC, respectively. By omitting a trials factor in our analysis, we obtain a conservative upper limit on the sensitive $\langle VT \rangle$ of the searches. Though MBTA and PyCBC results use the full injection set, GstLAL analysed a subset; the uncertainties in $\langle VT \rangle$ shown in Fig. 1 are therefore larger for GstLAL.

To lowest order, the inspiral of a binary depends sensitively on the chirp mass of the system (Blanchet 2014), which is defined as $\mathcal{M} \equiv (m_1 m_2)^{3/5} / (m_1 + m_2)^{1/5}$. Therefore, we split the population into nine equally spaced chirp mass bins in the range $0.16 \leq \mathcal{M} \leq 2.72 M_\odot$ to determine the $\langle VT \rangle$ as a function of the chirp mass, shown in Fig. 1. The highest chirp mass bin of this search exhibits a drop in sensitivity as the component masses contained within this bin are beyond the redshifted component masses covered by the template bank (Section 2). As a consequence, there is a drop in efficiency and smaller $\langle VT \rangle$ values in that region. The sensitivity estimates obtained from the analysis of O3a data with the common injection set are consistent with the ones reported in our previous work (Abbott et al. 2022).

The null result from O3 yields $\langle VT \rangle$ values approximately two times larger than those obtained for O3a, in agreement with the expected increase in observing time. The sensitive hypervolumes

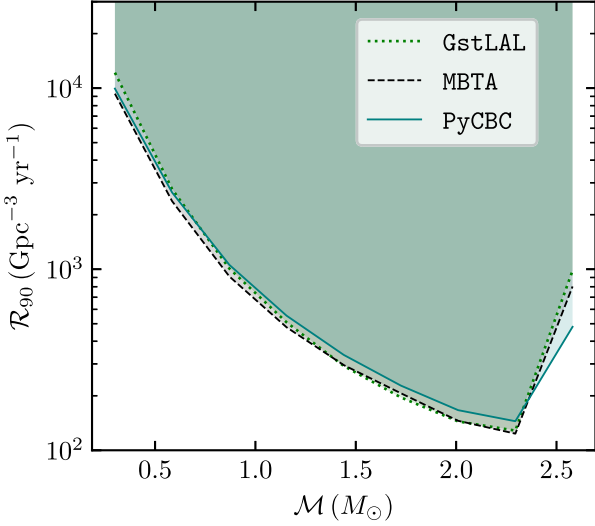


Figure 2. Merger rate limits as function of the source frame chirp mass of the binary system, in data from the full O3. The dotted, dashed, and solid lines represent the 90 per cent confidence limits obtained by GSTLAL, MBTA, and PyCBC, respectively.

of the searches presented in GWTC-3 (Abbott et al. 2021b) for chirp masses of 1.3 and 2.3 M_{\odot} are comparable to those in Fig. 1 even though the mass ratio bounds of the two populations are different.

Given the obtained sensitive volume and the absence of significant detection, one can infer merger rate limits. Treating each bin, i , as a different population, we computed an upper limit on the binary merger rate to 90 per cent confidence (Biswas et al. 2009):

$$\mathcal{R}_{90,i} = \frac{2.3}{\langle VT \rangle_i}. \quad (3)$$

We show in Figs 2 and 3 the upper limits on the binary merger rate as function of the chirp mass and in the source m_1 – m_2 plane, respectively.

4 CONSTRAINTS ON DARK MATTER MODELS

The upper limits that we infer from our null result can generically be used to constrain models that predict an observable population of binaries with at least one SSM component. We connect our results to two possible sources of SSM BHs: PBHs and DBHs. We parametrize our constraints in terms of the fraction of the DM that can be composed of compact objects under each model.

4.1 Primordial black holes

The abundance and mass distribution of PBHs depend on the details of their particular formation mechanism. The primordial power spectrum generated during inflation must have sufficiently large fluctuations on small scales for PBHs formation, while keeping the fluctuations small at the scale of the observed cosmic microwave background anisotropies (Cole et al. 2022). This is possible in several two-field models of inflation (Clesse & García-Bellido 2015; Braglia et al. 2020; Zhou et al. 2020; De Luca, Franciolini & Riotto 2021), single-field models with a non-slow-roll regime due to specific features in the inflation dynamics (García-Bellido & Ruiz Morales 2017; Ezquiaga, García-Bellido & Ruiz Morales 2018), and by the enhancement of fluctuations at small scales due to quantum diffusion (Pattison et al. 2017; Ezquiaga, García-Bellido & Vennin 2020),

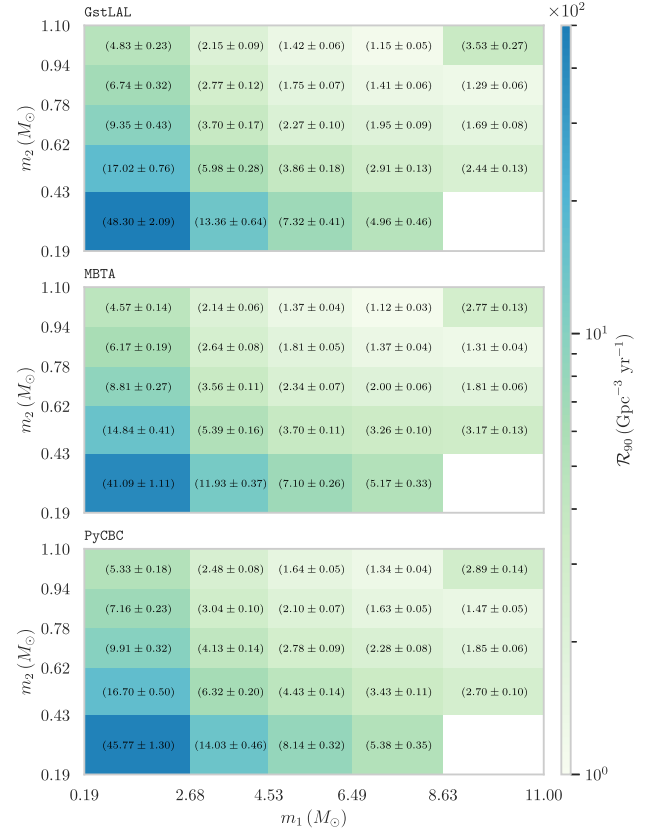


Figure 3. Merger rate limits in the source frame m_1 – m_2 plane, in data from the full O3 for the three pipelines. The error bars in each panel are given at the 90 per cent confidence interval, following equation (2).

which provide recent examples of inflationary scenarios that can produce PBHs in the SSM range.

The probability of matter fluctuations to collapse into PBHs is enhanced by the decrease of the radiation pressure as different particles become non-relativistic along the thermal history of the Universe (Carr et al. 2021a). In particular, a peak around a solar mass is expected due to the QCD transition, although its exact position and height depend on the characteristics of the matter fluctuations at those scales (Byrnes et al. 2018). Furthermore, the probability of binary formation and thus estimates of the event rates depends on the clustering of PBHs and the cluster dynamics. This remains an area of active study (Raidal et al. 2019; Jedamzik 2020; Trashorras, García-Bellido & Nesseris 2021). All these uncertainties make our predictions on the DM fraction of PBHs very sensitive to the particular choice of the model parameters (Franciolini et al. 2022; Escrivà, Bagui & Clesse 2023).

We update the theoretical merger rate of PBHs used in previous LVK searches (Abbott et al. 2018, 2019b, 2022). We approximate the merger rates of early PBH binaries (EBs) formed in the radiation-dominated era with the approximations provided by Hütsi et al. (2021), Chen & Huang (2018), Ali-Haïmoud, Kovetz & Kamionkowski (2017), and numerically validated with N -body simulations in Raidal et al. (2019),

$$\frac{d\mathcal{R}^{\text{PBH}}}{d \ln m_1 d \ln m_2} = 1.6 \times 10^6 \text{ Gpc}^{-3} \text{ yr}^{-1} \times f_{\text{sup}} f_{\text{PBH}}^{53/37} f(m_1) \times f(m_2) \left(\frac{m_1 + m_2}{M_{\odot}} \right)^{-32/37} \left[\frac{m_1 m_2}{(m_1 + m_2)^2} \right]^{-34/37}, \quad (4)$$

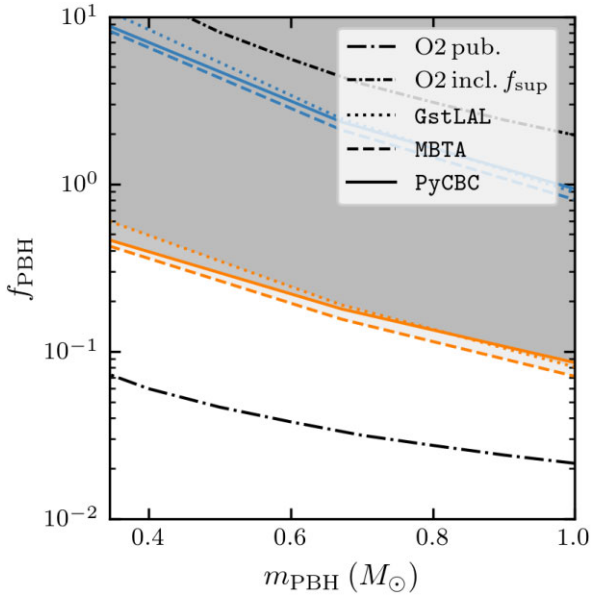


Figure 4. Constraints on DM fraction of PBHs, f_{PBH} , for a monochromatic mass function and assuming the merger rates for early PBH binaries from Hütsi et al. (2021) (orange) and late PBH binaries from Phukon et al. (2021) (blue). Shown in black are results for SSM searches in O2 (Abbott et al. 2019b) with and without the rate suppression factor f_{sup} . For the first time, $f_{\text{PBH}} = 1$ for early binaries is excluded in the whole SSM range probed by this search.

where f_{PBH} denotes the DM density fraction made of PBHs and $f(m)$ is the normalized PBH density distribution. We neglect the redshift dependence in the merger rates, since the current generation of ground-based interferometers is only sensitive to BBHs with at least one SSM component at low redshifts. The main difference, compared to the theoretical rates predicted by Sasaki et al. (2016) that were used in previous LVK searches, comes from a rate suppression factor f_{sup} that effectively accounts for PBH binary disruptions by early forming clusters due to Poisson fluctuations in the initial PBH separation, by matter inhomogeneities, and by nearby PBHs (Matsubara et al. 2019; Suyama & Yokoyama 2019). For instance, if PBHs have all the same mass or a strongly peaked mass function and significantly contribute to the DM, one gets $f_{\text{sup}} \approx 2.3 \times 10^{-3} f_{\text{PBH}}^{-0.65}$, so the merger rates are highly suppressed (Hütsi et al. 2021). As a result, the limits on f_{PBH} are much less stringent than previously estimated. Data from O2 still allow for $f_{\text{PBH}} = 1$ in a scenario where all the PBHs have the same mass. Though monochromatically distributed PBHs are unrealistic, they provide a useful approximation for models with a highly peaked distribution, e.g. as predicted from PBH scenarios with sharp QCD transitions (Carr et al. 2021a). Given the still large uncertainties and possible caveats for the merger rate prescriptions of early binaries, we also considered the case where merger rates entirely come from late PBH binaries (LBs) formed dynamically inside PBH clusters seeded by the above-mentioned Poisson fluctuations that grow in the matter-dominated era and lead to the formation of PBH clusters, following Clesse & Garcia-Bellido (2022) and Phukon et al. (2021). This allows us to illustrate the important variations in the PBH limits obtained for different binary formation scenarios.

For a monochromatic PBH mass distribution, we derive new limits on f_{PBH} in the SSM range, shown in Fig. 4, for both EBs and LBs. While the scenario of DM entirely made of PBHs with the same mass was not totally excluded by previous searches, after O3 it becomes strongly disfavored up to $1 M_{\odot}$, with $f_{\text{PBH}} < 0.6$ around $0.3 M_{\odot}$ and

$f_{\text{PBH}} < 0.09$ at $1 M_{\odot}$. For LBs only, we do not find yet significant limits, since we do not restrict f_{PBH} to be lower than 1.

For unequal mass BBH, the merger rates are more uncertain and model dependent, but one can obtain a limit on an effective parameter,

$$F_{\text{PBH}} \equiv \left(\frac{f_{\text{sup}}}{2.3 \times 10^{-3}} \right) f(m_1) f(m_2) f_{\text{PBH}}^{53/37}, \quad (5)$$

in such a way that it corresponds to the product of $f(m_2)$ and $f(m_1)$ in a scenario where $f_{\text{PBH}} \approx 1$. This allows us to establish model-independent limits on PBHs since F_{PBH} encompasses all the uncertainties on the mass distribution and rate suppression, by using the limits shown in Fig. 3 and the rates of equation (4) but neglecting their variations in individual mass bins. We find that the limits on F_{PBH} is sensitive to the location in the m_1 – m_2 plane. These can be used to constrain f_{PBH} for arbitrary mass functions. For models with $f_{\text{PBH}} = 1$ and a peak above $1 M_{\odot}$, these restrict the possible distribution of BHs in the SSM range. We find that some representative distributions with QCD-enhanced features (Byrnes et al. 2018; Carr et al. 2021a; De Luca et al. 2021; Jedamzik 2021) become constrained in the range $f_{\text{PBH}} \approx (0.1-1)$. SSM searches are therefore complementary to searches in the solar mass range in order to distinguish PBH mass functions that are viable from those that are more constrained.

4.2 Dark black holes

If all or some of the DM has rich enough particle content to dissipate kinetic energy and cool, then compact objects made from DM may form through gravitational collapse of the dark gas (Shandera et al. 2018). The particle content of the DM allows SSM BHs if, for example, there is a cosmologically dominant heavy fermion analogous to the proton but with mass greater than $938 \text{ MeV}/c^2$. In that case, the Chandrasekhar limit for DBHs is lower than that for Standard Model matter. Constraints on SSM BHs in mergers then constrain formation channels for DBHs in the detectable mass range, bounding the total cooling rate (total dissipation) of the dark sector (Singh et al. 2021).

Here we consider a population of DBHs formed within a particular dissipative scenario, the atomic DM model (Ackerman et al. 2009; Feng et al. 2009; Kaplan et al. 2010), with a power-law distribution of masses modelled after observations and simulations of Population III stars (Greif et al. 2011; Stacy & Bromm 2013; Hartwig et al. 2016). We derive the posterior probability for the fraction of dissipative DM that can be in BHs, the lower and upper limits of the DBH mass distribution, and the power-law slope, using the sensitive volume from the SSM search and modelled rates for DBH mergers (Shandera et al. 2018; Singh et al. 2021). The posterior is marginalized over the parameters that characterize the distribution, including the power-law slope and the upper limit of the distribution to obtain the constraints on the fraction of dissipative DM that can be in BHs, f_{DBH} , together with the lower limit of the DBH distribution $M_{\text{min}}^{\text{DBH}}$, as done in Singh et al. (2021) and Abbott et al. (2021a) previously.

The upper limits on f_{DBH} are shown as a function of $M_{\text{min}}^{\text{DBH}}$ in Fig. 5. Compared to the results obtained from the SSM search in O3a (Abbott et al. 2022), where the most stringent constraint on $f_{\text{DBH}} \lesssim 0.003$ per cent, the limit improves by roughly a factor of 2, which can be directly attributed to the increase in the observing time. We derive the strictest limit on $f_{\text{DBH}} \lesssim 0.0012-0.0014$ per cent at $M_{\text{min}}^{\text{DBH}} = 1 M_{\odot}$ across the three pipelines. The range of heavy dark fermion masses, m_{χ} probed by this search inferred from the Chandrasekhar limit of the fermionic particle progenitors of DBHs, is $1.1 < m_{\chi} < 8.9 \text{ GeV}/c^2$.

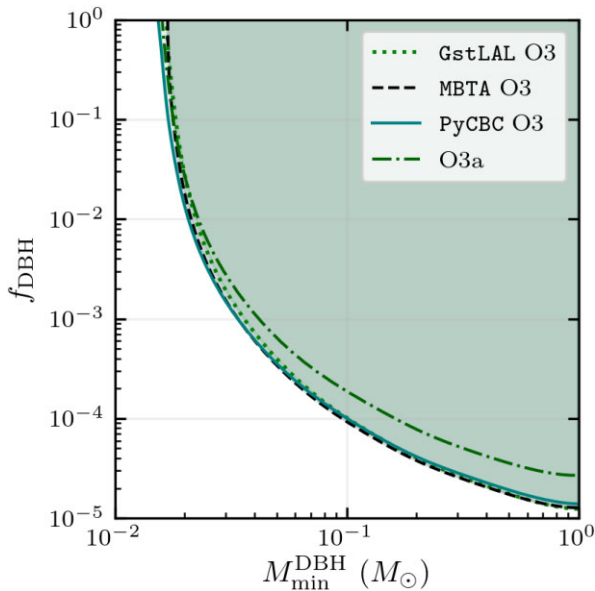


Figure 5. Constraints on the abundance of DBHs, f_{DBH} , as a function of the lower limit of the DBH mass distribution, $M_{\text{min}}^{\text{DBH}}$, from O3 data for the three search pipelines: GSTLAL (dotted), MBTA (dashed), and PyCBC (solid). Constraints from the search for SSM compact objects in O3a data (Abbott et al. 2022) are shown for comparison.

A non-detection provides no information for the model parameter $M_{\text{min}}^{\text{DBH}} < 2 \times 10^{-2} M_{\odot}$ because the searches are not sensitive enough to support distributions with $M_{\text{min}}^{\text{DBH}}$ in that mass range since we only consider $M_{\text{max}}^{\text{DBH}} = r M_{\text{min}}^{\text{DBH}}$ with $2 \leq r \leq 1000$. We also exclude limits where $M_{\text{min}}^{\text{DBH}} > 1 M_{\odot}$ because the detection of a SSM DBH would require a mass distribution with $M_{\text{min}}^{\text{DBH}} \leq 1 M_{\odot}$. If these limits survive with subsequent searches, the detection of a SSM compact object would directly constrain the particle properties of atomic DM. Future searches could potentially rule out regions of the DM parameter space associated with dissipative DM.

5 CONCLUSIONS AND OUTLOOK

We have presented a search for compact binary coalescences with at least one SSM component in data from the second half of the third LVK observing run, O3b. The search did not yield any significant candidates.

The absence of significant candidates enables us to set improved merger rate limits based on the full O3 data set. We obtain consistent results with each of the three considered search pipelines. We demonstrate how the new upper limits can be used to constrain two illustrative models: SSM PBHs and DBHs.

We have considered PBH merger rate models that incorporate additional physics relative to previous LVK works and obtained new limits that are less stringent than previous LVK searches for SSM objects. Using these upper limits, the data allow us to exclude equal mass PBHs with a DM fraction smaller than one, in the entire subsolar range probed by the search. More general PBH distributions with extended mass functions remain viable, even for $f_{\text{PBH}} \approx 1$. Our SSM search therefore provides limits that are complementary to other types of observations such as pulsar timing arrays (Chen, Yuan & Huang 2020; De Luca et al. 2021; Kohri & Terada 2021; Domènech & Pi 2022) and microlensing surveys (Allsman et al. 2001; Tisserand et al. 2007; Wyrzykowski et al. 2011) that can probe or constrain the GW

background induced by the density fluctuations at the origin of the formation of SSM PBHs.

For the dissipative DM model we consider bounds on DM self-interactions on large scales (Markevitch et al. 2004) already weakly constrain the amount of DM that can be efficiently cooling, so only some of the DM can have cooled sufficiently to form compact objects (Buckley & DiFranzo 2018; Shandera et al. 2018). Our analysis here provides the strongest constraint on this fraction so far from a SSM search, finding that no more than $f_{\text{DBH}} \approx 10^{-5}$ of atomic DM can be collapsed into BHs for distributions that include DBHs in the $0.2\text{--}1 M_{\odot}$ range where the sensitive volume is determined from this search alone.

Given the fundamental physics implications of observing a SSM BH, it will be important to continue this type of search in the next LVK observing runs (Abbott et al. 2020a). Each of the upcoming observing runs will be preceded by detector upgrades, designed to enhance the sensitivity of our ground-based interferometer network and our reach into the Universe. These developments will facilitate either the detection of a SSM compact object or provide tighter constraints on their abundance.

ACKNOWLEDGEMENTS

Analyses in this catalogue relied upon the LALSUITE software library (LIGO Scientific Collaboration 2018). The detection of the signals and subsequent significance evaluations in this catalogue were performed with the GSTLAL-based inspiral software pipeline (Messick et al. 2017; Sachdev et al. 2019; Hanna et al. 2020; Cannon et al. 2021), with the MBTA pipeline (Adams et al. 2016; Aubin et al. 2021), and with the PyCBC (Usman et al. 2016; Nitz et al. 2017; Davies et al. 2020) package. Plots were prepared with MATPLOTLIB (Hunter 2007). NUMPY (Harris et al. 2020) and SCIPY (Virtanen et al. 2020) were used in the preparation of the manuscript.

This material is based upon work supported by NSF’s LIGO Laboratory that is a major facility fully funded by the National Science Foundation. The authors also gratefully acknowledge the support of the Science and Technology Facilities Council (STFC) of the United Kingdom, the Max Planck Society (MPS), and the State of Niedersachsen/Germany for support of the construction of Advanced LIGO and construction and operation of the GEO 600 detector. Additional support for Advanced LIGO was provided by the Australian Research Council. The authors gratefully acknowledge the Italian Istituto Nazionale di Fisica Nucleare (INFN), the French Centre National de la Recherche Scientifique (CNRS), and the Netherlands Organisation for Scientific Research (NWO), for the construction and operation of the Virgo detector and the creation and support of the EGO consortium. The authors also gratefully acknowledge research support from these agencies and by the Council of Scientific and Industrial Research, India, the Department of Science and Technology, India, the Science & Engineering Research Board (SERB), India, the Ministry of Human Resource Development, India, the Spanish Agencia Estatal de Investigación (AEI), the Spanish Ministerio de Ciencia e Innovación and Ministerio de Universidades, the Conselleria de Fons Europeus, Universitat i Cultura and the Direcció General de Política Universitària i Recerca del Govern de les Illes Balears, the Conselleria d’Innovació, Universitats, Ciència i Societat Digital de la Generalitat Valenciana and the CERCA Programme Generalitat de Catalunya, Spain, the National Science Centre, Poland and the European Union – European Regional Development Fund, Foundation for Polish Science (FNP), the Swiss National Science Foundation (SNSF), the Russian

Foundation for Basic Research, the Russian Science Foundation, the European Commission, the European Social Fund (ESF), the European Regional Development Fund (ERDF), the Royal Society, the Scottish Funding Council, the Scottish Universities Physics Alliance, the Hungarian Scientific Research Fund (OTKA), the French Lyon Institute of Origins (LIO), the Belgian Fonds De la Recherche Scientifique (FRS-FNRS), Actions de Recherche Concertées (ARC) and Fonds Wetenschappelijk Onderzoek – Vlaanderen (FWO), Belgium, the Paris Île-de-France Region, the National Research, Development and Innovation Office Hungary (NKFIH), the National Research Foundation of Korea, the Natural Science and Engineering Research Council Canada, Canadian Foundation for Innovation (CFI), the Brazilian Ministry of Science, Technology, and Innovations, the International Center for Theoretical Physics South American Institute for Fundamental Research (ICTP-SAIFR), the Research Grants Council of Hong Kong, the National Natural Science Foundation of China (NSFC), the Leverhulme Trust, the Research Corporation, the Ministry of Science and Technology (MOST), Taiwan, the United States Department of Energy, and the Kavli Foundation. The authors gratefully acknowledge the support of the NSF, STFC, INFN, and CNRS for provision of computational resources. Funding for this project was provided by the Charles E. Kaufman Foundation of the Pittsburgh Foundation and the Penn State Institute for Computational and Data Sciences.

This work was supported by MEXT, JSPS Leading-edge Research Infrastructure Program, JSPS Grant-in-Aid for Specially Promoted Research 26000005, JSPS Grant-in-Aid for Scientific Research on Innovative Areas 2905: JP17H06358, JP17H06361, and JP17H06364, JSPS Core-to-Core Program A. Advanced Research Networks, JSPS Grant-in-Aid for Scientific Research (S) 17H06133 and 20H05639, JSPS Grant-in-Aid for Transformative Research Areas (A) 20A203: JP20H05854, the joint research program of the Institute for Cosmic Ray Research, University of Tokyo, National Research Foundation (NRF), Computing Infrastructure Project of KISTI-GSDC, Korea Astronomy and Space Science Institute (KASI), and Ministry of Science and ICT (MSIT) in Korea, Academia Sinica (AS), AS Grid Center (ASGC) and the Ministry of Science and Technology (MOST) in Taiwan under grants including AS-CDA-105-M06, Advanced Technology Center (ATC) of NAOJ, and Mechanical Engineering Center of KEK.

We would like to thank all of the essential workers who put their health at risk during the COVID-19 pandemic, without whom we would not have been able to complete this work.

DATA AVAILABILITY

The raw data used in the analyses are available via the Gravitational Wave Open Science Center. The derived data generated in this work can be found on the LIGO Document Control Center.

REFERENCES

- Aasi J. et al., 2015, *Classical Quantum Gravity*, 32, 074001
 Abbott B. et al., 2005, *Phys. Rev. D*, 72, 082002
 Abbott B. et al., 2008, *Phys. Rev. D*, 77, 062002
 Abbott B. P. et al., 2016a, *Phys. Rev. X*, 6, 041015
 Abbott B. P. et al., 2016b, *Phys. Rev. Lett.*, 116, 061102
 Abbott B. P. et al., 2018, *Phys. Rev. Lett.*, 121, 231103
 Abbott B. P. et al., 2019a, *Phys. Rev. X*, 9, 031040
 Abbott B. P. et al., 2019b, *Phys. Rev. Lett.*, 123, 161102
 Abbott B. et al., 2020a, *Living Rev. Relativ.*, 23, 3
 Abbott B. P. et al., 2020b, *Classical Quantum Gravity*, 37, 045006
 Abbott R. et al., 2020c, *Phys. Rev. Lett.*, 125, 101102
 Abbott B. et al., 2020d, *ApJ*, 892, L3
 Abbott R. et al., 2020e, *ApJ*, 896, L44
 Abbott R. et al., 2020f, *ApJ*, 900, L13
 Abbott R. et al., 2021a, preprint (arXiv:2108.01045)
 Abbott R. et al., 2021b, preprint (arXiv:2111.03606)
 Abbott R. et al., 2021c, *Phys. Rev. X*, 11, 021053
 Abbott R. et al., 2021d, *SoftwareX*, 13, 100658
 Abbott R. et al., 2021e, *ApJ*, 913, L7
 Abbott R. et al., 2022, *Phys. Rev. Lett.*, 129, 061104
 Abbott R. et al., 2023, *Phys. Rev. X*, 13, 011048
 Acernese F. et al., 2015, *Classical Quantum Gravity*, 32, 024001
 Ackerman L., Buckley M. R., Carroll S. M., Kamionkowski M., 2009, *Phys. Rev. D*, 79, 023519
 Adams T. et al., 2016, *Classical Quantum Gravity*, 33, 175012
 Aghanim N. et al., 2020, *A&A*, 641, A6
 Ajith P., 2011, *Phys. Rev. D*, 84, 084037
 Ali-Haïmoud Y., Kovetz E. D., Kamionkowski M., 2017, *Phys. Rev. D*, 96, 123523
 Allen B., 2005, *Phys. Rev. D*, 71, 062001
 Allen B., Anderson W. G., Brady P. R., Brown D. A., Creighton J. D. E., 2012, *Phys. Rev. D*, 85, 122006
 Allsman R. A. et al., 2001, *ApJ*, 550, L169
 Arun K. G., Buonanno A., Faye G., Ochsner E., 2009, *Phys. Rev. D*, 79, 104023
 Aubin F. et al., 2021, *Classical Quantum Gravity*, 38, 095004
 Bailyn C. D., Jain R. K., Coppi P., Orosz J. A., 1998, *ApJ*, 499, 367
 Barrow J. D., Copeland E. J., Kolb E. W., Liddle A. R., 1991, *Phys. Rev. D*, 43, 984
 Bean R., Magueijo J., 2002, *Phys. Rev. D*, 66, 063505
 Bird S., Cholis I., Muñoz J. B., Ali-Haïmoud Y., Kamionkowski M., Kovetz E. D., Raccanelli A., Riess A. G., 2016, *Phys. Rev. Lett.*, 116, 201301
 Biswas R., Brady P. R., Creighton J. D. E., Fairhurst S., 2009, *Classical Quantum Gravity*, 26, 175009
 Blanchet L., 2014, *Living Rev. Relativ.*, 17, 2
 Blanchet L., Damour T., Iyer B. R., Will C. M., Wiseman A. G., 1995, *Phys. Rev. Lett.*, 74, 3515
 Blanchet L., Damour T., Esposito-Farese G., Iyer B. R., 2005, *Phys. Rev. D*, 71, 124004
 Bohé A., Marsat S., Blanchet L., 2013, *Classical Quantum Gravity*, 30, 135009
 Bohé A., Faye G., Marsat S., Porter E. K., 2015, *Classical Quantum Gravity*, 32, 195010
 Braglia M., Hazra D. K., Finelli F., Smoot G. F., Sriramkumar L., Starobinsky A. A., 2020, *J. Cosmol. Astropart. Phys.*, 08, 001
 Bramante J., Elahi F., 2015, *Phys. Rev. D*, 91, 115001
 Bramante J., Linden T., 2014, *Phys. Rev. Lett.*, 113, 191301
 Bramante J., Linden T., Tsai Y.-D., 2018, *Phys. Rev. D*, 97, 055016
 Buckley M. R., DiFranzo A., 2018, *Phys. Rev. Lett.*, 120, 051102
 Buonanno A., Iyer B. R., Ochsner E., Pan Y., Sathyaprakash B. S., 2009, *Phys. Rev. D*, 80, 084043
 Byrnes C. T., Hindmarsh M., Young S., Hawkins M. R. S., 2018, *J. Cosmol. Astropart. Phys.*, 08, 041
 Cannon K. et al., 2021, *SoftwareX*, 14, 100680
 Carr B. J., Hawking S. W., 1974, *MNRAS*, 168, 399
 Carr B., Kühnel F., 2020, *Annu. Rev. Nucl. Part. Sci.*, 70, 355
 Carr B. J., Lidsey J. E., 1993, *Phys. Rev. D*, 48, 543
 Carr B., Clesse S., García-Bellido J., Kühnel F., 2021a, *Phys. Dark Universe*, 31, 100755
 Carr B., Kohri K., Sendouda Y., Yokoyama J., 2021b, *Rep. Progress Phys.*, 84, 116902
 Chandrasekhar S., 1931, *ApJ*, 74, 81
 Chandrasekhar S., 1935, *MNRAS*, 95, 207
 Chang J. H., Egana-Ugrinovic D., Essig R., Kouvaris C., 2019, *J. Cosmol. Astropart. Phys.*, 03, 036

- Chapline G. F., 1975, *Nature*, 253, 251
- Chen Z.-C., Huang Q.-G., 2018, *ApJ*, 864, 61
- Chen Z.-C., Yuan C., Huang Q.-G., 2020, *Phys. Rev. Lett.*, 124, 251101
- Chen Z.-C., Yuan C., Huang Q.-G., 2022, *Phys. Lett. B*, 829, 137040
- Choquette J., Cline J. M., Cornell J. M., 2019, *J. Cosmol. Astropart. Phys.*, 07, 036
- Clesse S., García-Bellido J., 2015, *Phys. Rev. D*, 92, 023524
- Clesse S., García-Bellido J., 2017, *Phys. Dark Universe*, 15, 142
- Clesse S., García-Bellido J., 2018, *Phys. Dark Universe*, 22, 137
- Clesse S., García-Bellido J., 2022, *Phys. Dark Universe*, 38, 101111
- Cole P. S., Gow A. D., Byrnes C. T., Patil S. P., 2022, preprint (arXiv:2204.07573)
- Cotner E., Kusenko A., 2017, *Phys. Rev. D*, 96, 103002
- Dal Canton T. et al., 2014, *Phys. Rev. D*, 90, 082004
- D'Amico G., Panci P., Lupi A., Bovino S., Silk J., 2018, *MNRAS*, 473, 328
- Damour T., Jaranowski P., Schaefer G., 2001, *Phys. Lett. B*, 513, 147
- Dasgupta B., Laha R., Ray A., 2021, *Phys. Rev. Lett.*, 126, 141105
- Davies G. S., Dent T., Tápai M., Harry I., McIsaac C., Nitz A. H., 2020, *Phys. Rev. D*, 102, 022004
- de Lavallaz A., Fairbairn M., 2010, *Phys. Rev. D*, 81, 123521
- De Luca V., Franciolini G., Riotto A., 2021, *Phys. Rev. Lett.*, 126, 041303
- Domènech G., Pi S., 2022, *Sci. China Phys. Mech. Astron.*, 65, 230411
- Ertl T., Woosley S. E., Sukhbold T., Janka H.-T., 2020, *ApJ*, 890, 51
- Escrivà A., Bagui E., Clesse S., 2023, *J. Cosmol. Astropart. Phys.*, 05, 004
- Essig R., Mcdermott S. D., Yu H.-B., Zhong Y.-M., 2019, *Phys. Rev. Lett.*, 123, 121102
- Ezquiaga J. M., García-Bellido J., Ruiz Morales E., 2018, *Phys. Lett. B*, 776, 345
- Ezquiaga J. M., García-Bellido J., Vennin V., 2020, *J. Cosmol. Astropart. Phys.*, 03, 029
- Farmer R., Renzo M., de Mink S. E., Marchant P., Justham S., 2019, *ApJ*, 887, 53
- Farr W. M., Sravan N., Cantrell A., Kreidberg L., Bailyn C. D., Mandel I., Kalogera V., 2011, *ApJ*, 741, 103
- Farrow N., Zhu X.-J., Thrane E., 2019, *ApJ*, 876, 18
- Feng J. L., Kaplinghat M., Tu H., Yu H.-B., 2009, *J. Cosmol. Astropart. Phys.*, 07, 004
- Fishbach M., Kalogera V., 2022, *ApJ*, 929, L26
- Franciolini G., Urbano A., 2022, *Phys. Rev. D*, 106, 123519
- Franciolini G., Musco I., Pani P., Urbano A., 2022, *Phys. Rev. D*, 106, 123526
- García-Bellido J., Ruiz Morales E., 2017, *Phys. Dark Universe*, 18, 47
- García-Bellido J., Linde A. D., Wands D., 1996, *Phys. Rev. D*, 54, 6040
- Garriga J., Vilenkin A., Zhang J., 2016, *J. Cosmol. Astropart. Phys.*, 02, 064
- Goldman I., Nussinov S., 1989, *Phys. Rev. D*, 40, 3221
- Greif T., Springel V., White S., Glover S., Clark P., Smith R., Klessen R., Bromm V., 2011, *ApJ*, 737, 75
- Hanna C. et al., 2020, *Phys. Rev. D*, 101, 022003
- Harris C. R. et al., 2020, *Nature*, 585, 357
- Harry I. W., Nitz A. H., Brown D. A., Lundgren A. P., Ochsner E., Keppel D., 2014, *Phys. Rev. D*, 89, 024010
- Hartwig T., Volonteri M., Bromm V., Klessen R. S., Barausse E., Magg M., Stacy A., 2016, *MNRAS*, 460, L74
- Hawking S., 1971, *MNRAS*, 152, 75
- Hippert M., Setford J., Tan H., Curtin D., Noronha-Hostler J., Yunes N., 2022, *Phys. Rev. D*, 106, 035025
- Hunter J. D., 2007, *Comput. Sci. Eng.*, 9, 90
- Hütsi G., Raidal M., Vaskonen V., Veermäe H., 2021, *J. Cosmol. Astropart. Phys.*, 03, 068
- Ivanov P., Naselsky P., Novikov I., 1994, *Phys. Rev. D*, 50, 7173
- Jedamzik K., 2020, *J. Cosmol. Astropart. Phys.*, 09, 022
- Jedamzik K., 2021, *Phys. Rev. Lett.*, 126, 051302
- Juan J. I., Serpico P. D., Franco Abellán G., 2022, *J. Cosmol. Astropart. Phys.*, 07, 009
- Kaplan D. E., Krnjaic G. Z., Rehermann K. R., Wells C. M., 2010, *J. Cosmol. Astropart. Phys.*, 05, 021
- Kashlinsky A., 2016, *ApJ*, 823, L25
- Khlopov M. Y., 2010, *Res. Astron. Astrophys.*, 10, 495
- Khlopov M., Malomed B. A., Zeldovich I. B., 1985, *MNRAS*, 215, 575
- Kim H. I., Lee C. H., 1996, *Phys. Rev. D*, 54, 6001
- Kohri K., Terada T., 2021, *Phys. Lett. B*, 813, 136040
- Kouvaris C., Tinyakov P., 2011, *Phys. Rev. D*, 83, 083512
- Kouvaris C., Tinyakov P., Tytgat M. H. G., 2018, *Phys. Rev. Lett.*, 121, 221102
- Latif M., Lupi A., Schleicher D., D'Amico G., Panci P., Bovino S., 2019, *MNRAS*, 485, 3352
- LIGO Scientific Collaboration, 2018, *LIGO Algorithm Library*. <http://dx.doi.org/10.7935/GT1W-FZ16>
- Magee R. et al., 2019, *ApJ*, 878, L17
- Mandel I., Farmer A., 2022, *Phys. Rep.*, 955, 1
- Markevitch M., Gonzalez A. H., Clowe D., Vikhlinin A., Forman W., Jones C., Murray S., Tucker W., 2004, *ApJ*, 606, 819
- Matsubara T., Terada T., Kohri K., Yokoyama S., 2019, *Phys. Rev. D*, 100, 123544
- Messick C. et al., 2017, *Phys. Rev. D*, 95, 042001
- Mikóczy B., Vasuth M., Gergely L. A., 2005, *Phys. Rev. D*, 71, 124043
- Mishra C. K., Kela A., Arun K. G., Faye G., 2016, *Phys. Rev. D*, 93, 084054
- Müller B. et al., 2019, *MNRAS*, 484, 3307
- Nitz A. H., Wang Y.-F., 2021a, *ApJ*, 915, 54
- Nitz A. H., Wang Y.-F., 2021b, *Phys. Rev. Lett.*, 126, 021103
- Nitz A. H., Wang Y.-F., 2021c, *Phys. Rev. Lett.*, 127, 151101
- Nitz A. H., Wang Y.-F., 2022, *Phys. Rev. D*, 106, 023024
- Nitz A. H., Dent T., Dal Canton T., Fairhurst S., Brown D. A., 2017, *ApJ*, 849, 118
- Nitz A. H., Capano C., Nielsen A. B., Reyes S., White R., Brown D. A., Krishnan B., 2019a, *ApJ*, 872, 195
- Nitz A. H. et al., 2019b, *ApJ*, 891, 123
- Nitz A. H., Kumar S., Wang Y.-F., Kastha S., Wu S., Schäfer M., Dhurkunde R., Capano C. D., 2023, *ApJ*, 946, 59
- Nitz A. H., Capano C. D., Kumar S., Wang Y.-F., Kastha S., Schäfer M., Dhurkunde R., Cabero M., 2021, *ApJ*, 922, 76
- Olsen S., Venumadhav T., Mushkin J., Roulet J., Zackay B., Zaldarriaga M., 2022, *Phys. Rev. D*, 106, 043009
- Owen B. J., 1996, *Phys. Rev. D*, 53, 6749
- Ozel F., Psaltis D., Narayan R., McClintock J. E., 2010, *ApJ*, 725, 1918
- Pattison C., Vennin V., Assadullahi H., Wands D., 2017, *J. Cosmol. Astropart. Phys.*, 10, 046
- Phukon K. S. et al., 2021, preprint (arXiv:2105.11449)
- Poisson E., 1998, *Phys. Rev. D*, 57, 5287
- Raidal M., Spethmann C., Vaskonen V., Veermäe H., 2019, *J. Cosmol. Astropart. Phys.*, 02, 018
- Ryan M., Gurian J., Shandera S., Jeong D., 2022, *ApJ*, 934, 120
- Sachdev S. et al., 2019, preprint (arXiv:1901.08580)
- Sasaki M., Suyama T., Tanaka T., Yokoyama S., 2016, *Phys. Rev. Lett.*, 117, 061101
- Sathyaprakash B. S., Dhurandhar S. V., 1991, *Phys. Rev. D*, 44, 3819
- Shandera S., Jeong D., Gebhardt H. S. G., 2018, *Phys. Rev. Lett.*, 120, 241102
- Singh D., Ryan M., Magee R., Akhter T., Shandera S., Jeong D., Hanna C., 2021, *Phys. Rev. D*, 104, 044015
- Spera M., Trani A. A., Mencagli M., 2022, *Galaxies*, 10, 76
- Stacy A., Bromm V., 2013, *MNRAS*, 433, 1094
- Suwa Y., Yoshida T., Shibata M., Umeda H., Takahashi K., 2018, *MNRAS*, 481, 3305
- Suyama T., Yokoyama S., 2019, *Progress Theor. Exp. Phys.*, 2019, 103E02
- Takhistov V., 2018, *Phys. Lett. B*, 782, 77
- Takhistov V., Fuller G. M., Kusenko A., 2021, *Phys. Rev. Lett.*, 126, 071101
- Tisserand P. et al., 2007, *A&A*, 469, 387
- Tiwari V., 2018, *Classical Quantum Gravity*, 35, 145009
- Trashorras M., García-Bellido J., Nesseris S., 2021, *Universe*, 7, 18
- Usman S. A. et al., 2016, *Classical Quantum Gravity*, 33, 215004

- Venumadhav T., Zackay B., Roulet J., Dai L., Zaldarriaga M., 2019, *Phys. Rev. D*, 100, 023011
- Venumadhav T., Zackay B., Roulet J., Dai L., Zaldarriaga M., 2020, *Phys. Rev. D*, 101, 083030
- Villanueva-Domingo P., Mena O., Palomares-Ruiz S., 2021, *Frontiers Astron. Space Sci.*, 8, 87
- Virtanen P. et al., 2020, *Nat. Methods*, 17, 261
- Woosley S. E., 2017, *ApJ*, 836, 244
- Wyrzykowski L. et al., 2011, *MNRAS*, 416, 2949
- Zel'dovich Y. B., Novikov I. D., 1967, *SvA*, 10, 602
- Zevin M., Spera M., Berry C. P. L., Kalogera V., 2020, *ApJ*, 899, L1
- Zhou Z., Jiang J., Cai Y.-F., Sasaki M., Pi S., 2020, *Phys. Rev. D*, 102, 103527

SUPPORTING INFORMATION

Supplementary data are available at *MNRAS* online.

M2200018.tex
M2200018.pdf

Please note: Oxford University Press is not responsible for the content or functionality of any supporting materials supplied by the authors. Any queries (other than missing material) should be directed to the corresponding author for the article.

This paper has been typeset from a $\text{\TeX}/\text{\LaTeX}$ file prepared by the author.